
DProtoNet: Decoupling Prototype Activation via Multiple Dynamic Masks

Yitao Peng, Yihang Liu, Longzhen Yang, Lianghua He*
College of Electronic and Information Engineering Tongji University
4800 Cao'an Highway, Shanghai, China 201804
{pyt, 2111131, yanglongzhen, helianghua}@tongji.edu.cn

Abstract

The interpretability of neural networks has recently received extensive attention. The previous prototype-based explainable networks involved prototype activation in both the reasoning process and interpretation process, which requires specific explainable structures for the prototype. This makes the network less accurate as it gains interpretability. To avoid this problem, we propose a new model: decoupling prototypical network (DProtoNet), which contains three modules. 1) encoder module: we propose unrestricted masks to generate expressive features and prototypes. 2) inference module: we propose a multi-image prototype learning method to update prototypes so that the network can learn generalized prototypes. 3) interpretation module: we propose multiple dynamic masks (MDM) decoder to explain the network, which generates heatmaps using the consistent activation of the original image and mask image at the detection nodes of the network. It decouples the inference module and interpretation module of a prototype-based network by avoiding the use of prototype activation to explain the network's decisions, so that the accuracy and interpretability of the network can be simultaneously improved. We test on multiple public general and medical datasets. The accuracy of our method is improved compared with the previous methods, which can be improved by up to 5%. DProtoNet achieves state-of-the-art interpretability.

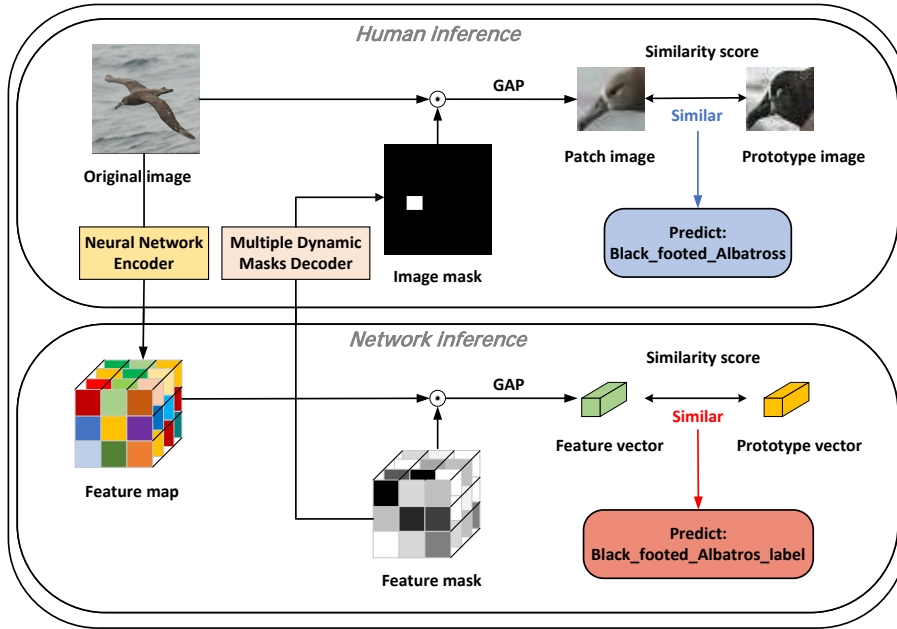


Figure 1: The decision-making process of humans and DProtoNet.

1 Introduction

With the continuous development of neural networks [23, 10, 5, 15, 16, 27], the interpretability of neural networks is a research direction that has received extensive attention. How to make neural networks have good classification performance and good interpretability at the same time is a challenging task. A large number of interpretability methods have been proposed.

Saliency maps [22, 18, 32, 26, 1, 29, 21] use localization as an explanation for predictions, but this only provides the network’s area of interest for a given image, which does not fully represent the way the network makes its decisions [20]. They lack generality and are not easily transferable to neural networks with non-convolutional architecture.

Interpretable models [2, 25, 24, 11, 8, 14] are designed to function in a human-comprehensible way [20]. They enable the network to learn feature templates for each class in the dataset, called prototypes. They predict the corresponding class by finding prototypes that are similar to the class. ProtoPNet [2], GenProtoPNet [24] and XProtoNet [11] uses patches of different sizes in feature maps as prototypes for classification. However, none of these methods [2, 25, 24, 11] fully extract the information of feature map. In order to make the prototype extracted by the network interpretable, they set a specific prototype structure, which makes the network subject to spatial constraints, which in turn leads to the reduction of network accuracy. These prototype-based networks [2, 25, 24,

11] think: “The patch of input image that corresponds to the prototype should be the one that the prototype activates the most strongly on.” [2] They localize prototypes and decision regions by upsampling feature maps with similarity activation maps produced by prototypes, and then looking for high activation regions as class activation maps (CAM) in the upsampled images. There is no complete theory to support that the activation area of the activation map can correspond to the decision area in the original image, so the visualization generated by the previous method is not well interpretable, and the positioning ability is not accurate.

In this paper, we propose DProtoNet to mine prototypes in data for interpretable classification. It uses the unrestricted masks to extract the information in the feature map and relieve the constraints of the specific structure of the prototype on the latent space of the network. We introduce multi-image prototype learning to update the prototype by mixing the same prototype features mined on multiple images, so that the prototype can be represented as a distribution of certain types of features, avoiding the problem of introducing noisy prototypes when the image or network performance is low quality. By generalizing the extraction and learning of prototypes, DProtoNet enhances the expressive ability of prototypes and improves the classification performance of the network.

In order to solve the above problems of inaccurate localization of CAM and lack theoretical support. We propose MDM decoder to visualize the decision regions of the network and give a mathematical proof. We think that when the network analyzes the image, only the decision region will promote the activation value of the network at the specific node, and the region unrelated to the decision will not affect the activation value of the network even if it is masked. Therefore, MDM decoder sets detection nodes in the network, learns vectors through the consistent activation of the original image and the mask image on the detection nodes. The previous mask-based methods [6, 3, 31] only perform activation-consistent learning for mask the same size as the original image, which is prone to adversarial effects [18]. To reduce this, MDM decoder stacks upsampled masks from multiple vectors of different sizes to generate the CAM. The mask generated by MDM decoder can better preserve the spatial and semantic information of the decision regions. We set the prototype node in DProtoNet as the detection node, which can accurately locate the image information corresponding to the prototype and the decision region of DProtoNet.

As shown in Figure 1, the DProtoNet keep the prototype-based inference architecture, and use the MDM decoder to explain the prototype and decision regions of DProtoNet. It decouples the inference module and the interpretation module of the network, which relieves the mutual constraints of accuracy and interpretability on network performance, and improves the accuracy and interpretability of the network.

The key contributions of our work are:

- We propose unrestricted masks to mine global information from feature maps, thereby improving the expressiveness of features and prototypes.
- We propose multi-image prototype learning by which generalized proto-

types can be learned.

- We propose a general, interpretable and powerful method MDM decoder for finding basis for classification decisions in neural networks. We give a mathematical proof of the feasibility of it.
- We propose a new model DProtoNet, which incorporates unrestricted mask, multi-image prototype learning, and MDM decoder into encoder, inference, and interpretation modules. This allows the model to have good interpretability while improving accuracy.

2 Related Work

2.1 Saliency Maps

Saliency methods produce a visual interpretation map that represent the importance of image pixels for network classification. Class activation mapping is a pioneering saliency method [17]. [32] uses Global Average Pooling (GAP) to integrate information from all features to obtain CAM. To address the limitation that CAM can only be used for specific mode structures, Grad-CAM [21] utilizes the gradient information of convolutional layers to obtain CAM. [1] proposes Grad-CAM++ to add an extra weight to measure the elements of the gradient map to precisely locate the CAM. To improve the versatility and accuracy of CAM, Score-CAM [29] represents a gradient-free method for activation maps in an intuitive and understandable way. Ablation-CAM [19] analyzes the contribution of each factor to the network. These methods are various post-hoc attempts to interpret an already trained model, they only show the regions the network looks at in a given image. And these methods lack generality. Therefore, we propose a method to indicate the decision regions of the network, which can provide good interpretability for any structure of the network.

2.2 Interpretable Models

Setting the structure of the neural network to mimic the human reasoning process makes the network interpretable. ProtoPNet [2] takes 1×1 patches of feature maps as prototypes and uses them for classification. NP-ProtoPNet [25] fixes the last classification layer and exploits negative reasoning to improve the classification performance. To improve the adaptability of prototypes for different tasks, [24] proposed Gen-ProtoPNet, which improves the representation ability of the prototype by setting the prototype as the $h \times w$ patch on the feature map. [11] proposed XProtoNet, which sets the prototype as a feature vector with variable activation positions and sizes. These works set a specific shape for the prototype to limit the expressive ability of the network, and the method of using the prototype activation map as an explanation has lacks theoretical support and interpretability. Therefore, we set up a decoupled network

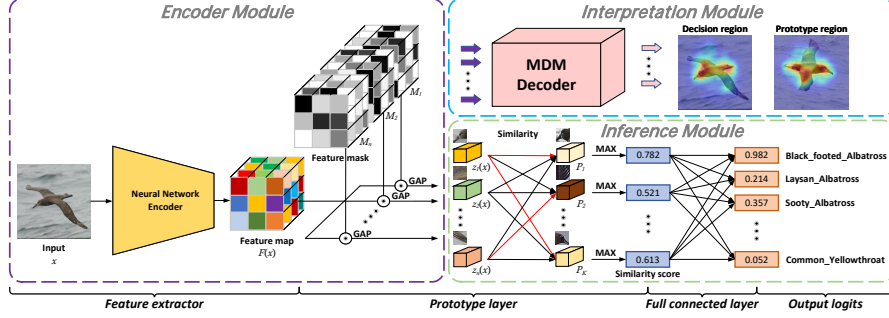


Figure 2: Overall architecture of DProtoNet. DProtoNet distinguishes image categories by comparing the features of an input image to the prototypes of each classification. DProtoNet generates decision region and prototype region for reference through the MDM decoder.

architecture, which make the network maintain the accuracy of the backbone network and have great interpretability.

3 Methodology

Figure 2 shows the overall architecture of our proposed framework DProtoNet, which consists of: the feature extractor, prototype layer, full connected layer, output logits and MDM decoder. It can also be divided into three modules: encoder, inference and interpretation. We describe the inference and training of DProtoNet in Section 3.1, and explain in Section 3.2 how to extract features within a global region. In Section 3.3, we describe prototype update method. We introduce how to use multiple dynamic masks decoder to find the basis for decisions in Section 3.4.

3.1 Inference and Training of DProtoNet

Classification Process. Let: DProtoNet has K prototypes, input image $x \in R^{H \times W \times C}$, prototype P_j . Feature extractor is composed of a backbone network f_b and a shaping network f_a . x passes f_b , f_a to get feature map $F(x) \in R^{H_1 \times W_1 \times D}$, the feature extractor extracts the feature vector $z_i(x)$. Similar to previous models [2, 25, 24], it calculates a similarity score between $z_i(x)$ and P_j , activation $g_{p_j}(x)$ and logit $p(y^c|x)$.

$$s(z_i(x), P_j) = \|z_i(x) - P_j\|_2^2 \quad (1)$$

$$g_{p_j}(x) = g(F(x), P_j) = \max_{1 \leq i \leq n} \log\left(\frac{s(z_i(x), P_j) + 1}{s(z_i(x), P_j) + \epsilon}\right) \quad (2)$$

$$p(y^c|x) = \sum_{j=1}^K w_j^c g(F(x), P_j) \quad (3)$$

Where weight w_j^c indicates how important each prototype P_j is for the class c , ϵ prevents division by zero.

Training Scheme. Let training images is $\{(x_i, y_i)\}_{i=1}^n$, which has m classes. Q_k represents the set of prototype p_j belonging to class k , $w_h^{(u,v)}$ be the (u,v) -th entry in w_h that corresponds to the weight connection between the output of the v -th prototype unit g_{p_v} and the logit of class u .

$$L = \frac{1}{n} \sum_{i=1}^n \text{CrsEnt}(f_h \circ g_p \circ F(x_i), y_i) + \lambda_1 \text{Clst} + \lambda_2 \text{Sep} + \lambda_3 l_{w_h} \quad (4)$$

where Clst , Sep and l_{w_h} are defined by:

$$\text{Clst} = \frac{1}{n} \sum_{i=1}^n \min_{j:p_j \in Q_{y_i}} \min_k \|z_k(x_i) - p_j\|_2^2 \quad (5)$$

$$\text{Sep} = -\frac{1}{n} \sum_{i=1}^n \min_{j:p_j \notin Q_{y_i}} \min_k \|z_k(x_i) - p_j\|_2^2 \quad (6)$$

$$l_{w_h} = \sum_{u=1}^m \sum_{v:p_v \notin Q_u} |w_h^{(u,v)}| \quad (7)$$

The cross-entropy loss (CrsEnt) penalizes misclassification. The clustering cost minimization (Clst) encourages each image to have some latent feature regions that are at least close to a prototype of its own class. The separation cost minimization (Sep) encourages each latent patch of the image to be far away the prototypes of its own class. By optimizing l_{w_h} , the prototypes that only belong to the u class participate in the classification. Similar to the train stage in ProtoPNet [2], we train DProtoNet by optimizing L .

3.2 Extraction of Prototype with Feature Mask

We randomly generate feature masks $\{M_i\}_{i=1}^n$, $M_i \in R^{H_1 \times W_1 \times D}$, each value in the elements of $M_i \in [0, 1]$. Such as (8) generate feature vector z_i . Figure 3 shows the similarity score of the DProtoNet calculation process.

$$z_i(x) = \text{GAP}(M_i F(x)) \quad (8)$$

We use an unrestricted mask M_i to mine global information in the feature map. The set of prototypes that M_i can generate includes the set of prototypes generated by the previous models [2, 25, 24, 11]. In fact, if the previous models can mine at most $|Z|$ distinct feature vectors from $F(x)$, DProtoNet can mine

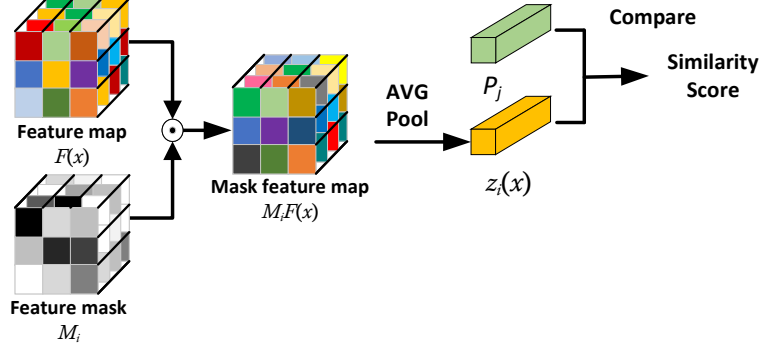


Figure 3: Similarity score of the DProtoNet calculation process.

at least $|Z|^D$ distinct feature vectors from $F(x)$. The expression ability of the prototype generated by M_i is far greater than that of the previous models.

Due to the arbitrariness of M_i , the information of $F(x)$ is preserved to the greatest extent, which relieves the spatial limitation of the prototype structure on the network and keeps the fitting ability of the backbone network unchanged. M_i is versatile, we are able to generate prototypes with any custom number and style, and can generate prototypes in the original picture through M_i and subsequent MDM decoder, preserving the interpretability of the network.

3.3 Multi-image Prototype Learning

We use a multi-image prototype learning method to update the prototype. Let: image x_i belongs class k , $\{x_i^1, x_i^2, \dots, x_i^R\}$ is a group of images generated by x_i is the original image after data augmentation. We believe that the original data x_i has the same characteristics as the data-augmented x_i^r ($r \in \{1, 2, \dots, R\}$). We sum and project the patches most similar to the prototype p_j in each x_i^r as update of p_j . Mathematically, for prototype p_j of class k , i.e., $p_j \in Q_k$, we perform the following update:

$$e_r = \underset{e}{\operatorname{argmin}} \|z_e(x_i^r) - p_j\|_2 \quad (9)$$

$$p_j \leftarrow \underset{p}{\operatorname{argmin}} \sum_{r=1}^R \|z_{e_r}(x_i^r) - p\|_2^2 \quad (10)$$

The p_j generated by mixing multiple images is more robust than the p_j generated by a single image. From (10), according to the derivation, it can be known that the p_j update formula is:

$$p_j = \frac{1}{R} \sum_{r=1}^R z_{e_r}(x_i^r) \quad (11)$$

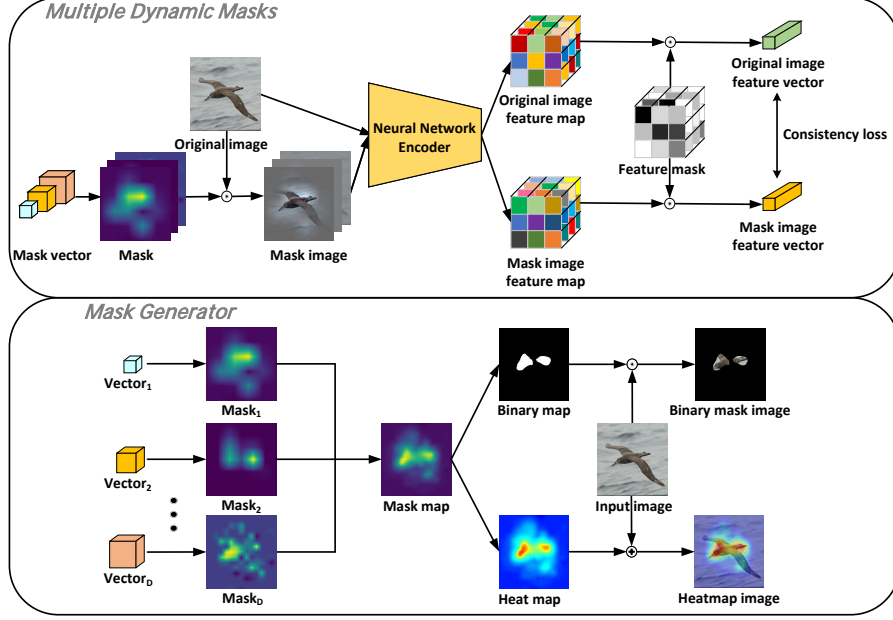


Figure 4: The flow of Multiple Dynamic Masks Decoder to generate saliency maps.

3.4 Multiple Dynamic Masks Decoder

As shown in Figure 4, it consists of Multiple Dynamic Masks (MDM) and Mask Generator. Multiple Dynamic Masks learn mask vectors of different sizes by constraining the original and mask images to have consistent activation values at the detection nodes of the neural network and mask vector values. Mask Generator mixes the upsampled mask vectors to generate CAM to point out the decision regions of the neural network. In DProtoNet, we choose the prototype nodes in the network as detection nodes.

Multiple Dynamic Masks. We propose activation-consistent learning of the network through masks generated by multiple vectors of different sizes. The mask vector size is inversely proportional to its receptive field.

Mask vectors $\{d_i\}_{i=1}^D$, $d_i \in R^{a_i \times b_i \times 1}$, d_i initialized to a fixed value τ . For any $i, j \in \{1, 2, \dots, D\}$, if $i \neq j$ then $a_i \neq a_j$ or $b_i \neq b_j$. Upsample function $g(\cdot)$, $g(d_i) \in R^{H \times W \times 1}$, d_i is upsampled to $g(d_i)$ to mask the image.

Note: For input image x , DProtoNet classifies x as c and p_t as a prototype belonging to c class. x^{p_t} is the image projected as p_t , and the corresponding mask is $M_{j_{p_t}}$. The feature mask of $z_j(x)$ with the smallest similarity score to p_t is M_{j_x} . $\{d_i^x\}_{i=1}^D$ and $\{d_i^{x^{p_t}}\}_{i=1}^D$ represent the mask vectors generated based

on x and x^{p_t} , respectively.

$$j_x = \underset{j}{\operatorname{argmin}} \|z_j(x) - p_t\|_2 \quad (12)$$

Figure 4 shows that we train $d_i^x, d_i^{x^{p_t}}$ by the activation consistency between the mask image and the original image. Train $d_i^x, d_i^{x^{p_t}}$ by minimizing the losses $L_i^x, L_i^{x^{p_t}}$.

$$L_i^x = s(z_{j_x}(g(d_i^x)x), z_{j_x}(x)) + \eta_i \sum_{u=1}^{a_i} \sum_{v=1}^{b_i} \frac{|d_{iuv}^x|}{|a_i b_i|} \quad (13)$$

$$L_i^{x^{p_t}} = s(z_{j_{p_t}}(g(d_i^{x^{p_t}})x^{p_t}), p_t) + \eta_i \sum_{u=1}^{a_i} \sum_{v=1}^{b_i} \frac{|d_{iuv}^{x^{p_t}}|}{|a_i b_i|} \quad (14)$$

Where η_i is a regularization factor. The mask vector retains the attention information of the image decision through the above optimizations.

Mask Generation. The trained $\{d_i^x\}_{i=1}^D$ and $\{d_i^{x^{p_t}}\}_{i=1}^D$ are upsampled to the original image size and mixed to generate CAM. Let A^x and $A^{x^{p_t}}$ are the CAMs of $z_{j_x}(x)$ and p_j in x and x^{p_t} .

$$A^x = N(\{\sum_{i=1}^D g(d_i^x) \geq \gamma\} \sum_{i=1}^D g(d_i^x)) \quad (15)$$

$$A^{x^{p_t}} = N(\{\sum_{i=1}^D g(d_i^{x^{p_t}}) \geq \gamma\} \sum_{i=1}^D g(d_i^{x^{p_t}})) \quad (16)$$

Where γ is threshold, $\{\cdot\}$ represents a truth-valued function, 1 if true, 0 otherwise. $N(X) = \frac{X - \min(X)}{\max(X) - \min(X)}$ is the normalization function.

As shown in Figure 4, we generate binary mask image and heatmap image by multiplying and stacking the CAM and the original image.

$$A_h^x = \alpha x + \beta A^x, A_h^{x^{p_t}} = \alpha x^{p_t} + \beta A^{x^{p_t}} \quad (17)$$

$$A_b^x = A^x x, A_b^{x^{p_t}} = A^{x^{p_t}} x^{p_t} \quad (18)$$

Where α, β are hyperparameters for image blending. A_h^x and $A_h^{x^{p_t}}$ are the heatmap images of x and x^{p_t} . A_b^x and $A_b^{x^{p_t}}$ are the binary mask images of x and x^{p_t} . They show the regions of the prototype and the regions of the prototype-like features in the images x^{p_t} and x , telling us the regions of interest for DProtoNet classification and the regions of the prototype images used for reference. This allows people to understand the decision-making process of DProtoNet.

Feasibility of Multiple Dynamic Masks. Let: z represents the region in image x , and $f_p(z)$ represents the activation of the neural network f at p when the data of the region z is taken as an input. $I(z) = k f_p(z)$, where k is a constant greater than zero, $I(z) \in [0, 1]$. $I(z)$ represents the amount of

information that region z contributes to the activation of neural network f at position p .

(13), (14) It can be abbreviated as the following formula:

$$L(m, z) = [f_p(z) - f_p(mz)]^2 + \eta m \quad (19)$$

Where z is all areas of d_i , and m is the corresponding mask value on it, $m \in [0, 1]$.

There are two public cognitions. When the corresponding regions on the original image do not intersect, it is considered that information I of the contribution of the two regions to activation f_p is irrelevant. And the greater the contribution of the investigation area to the activation, the greater the contribution to the information increment. Mathematically, z_1 and z_2 are the two regions of d_i , $i \in \{1, 2, \dots, N\}$, g is the upsampling function.

if $g(z_1) \cap g(z_2) = \emptyset$, then

$$I(z_1 + z_2) = I(z_1) + I(z_2) \quad (20)$$

if $I(z_1) < I(z_2)$, then

$$0 \leq \frac{\partial I(mz_1)}{\partial m} < \frac{\partial I(mz_2)}{\partial m} \quad (21)$$

Let: z_1 and z_2 represent any two disjoint regions of d_i ; m_1 , m_2 are mask value on z_1 , z_2 . From (20) and (21), the following conclusion can be proved, when $L(m, z)$ achieves the minimum value (See Supporting Materials for proof details).

$$(I(z_1) - I(z_2))(m_1 - m_2) \geq 0 \quad (22)$$

It can be seen from (22) that optimization (19) can make the mask satisfy: the higher the mask value of the region with higher decision contribution, the more image information is retained; the lower the mask value of the region with lower decision contribution, the less image information is retained. In DProtoNet, we select the prototype region as the activation region p so that the mask can mine the region represented by the prototype in the image.

4 Experiments

4.1 Datasets and Baselines

Datasets. We conduct experiments on four image recognition datasets, including two general image datasets CUB200-2011 [28], Stanford Cars [12] and two medical image datasets iChallenge-PM [7], RSNA [30]. We compare the accuracy of interpretable networks and backbone networks on the above four datasets. In the test dataset of CUB200-2011, 10 images are randomly selected for each class, constituting a total of 2000 images. We will compare the Recognition [29] and Localization [29] ability of the CAM generation method on these images.

Method	ResNet50	VGG19	DenseNet121
ProtoPNet [2]	78.1	76.3	80.4
NP-ProtoPNet [25]	71.3	75.6	76.2
Gen-ProtoPNet [24]	76.5	76.2	78.4
XProtoNet [11]	79.2	77.2	80.8
DProtoNet(ours)	80.9	77.9	81.3
CUB200-2011 $\uparrow\uparrow$, Stanford Cars $\downarrow\downarrow$ (datasets)			
ProtoPNet [2]	85.9	87.7	86.9
NP-ProtoPNet [25]	83.2	85.2	83.6
Gen-ProtoPNet [24]	85.6	85.8	84.1
XProtoNet [11]	84.7	87.3	84.3
DProtoNet(ours)	86.5	89.2	89.3

Table 1: Comparison results on general datasets.

Method	Datasets	Accuracy	Sensitivity
ProtoPNet [2]	RSNA	73.2	35.5
NP-ProtoPNet [25]	RSNA	76.4	28.1
Gen-ProtoPNet [24]	RSNA	76.9	34.8
XProtoNet [11]	RSNA	77.1	45.6
DProtoNet(ours)	RSNA	82.2	49.8
ProtoPNet [2]	iChallenge-PM	98	18.5
NP-ProtoPNet [25]	iChallenge-PM	97.25	0.4
Gen-ProtoPNet [24]	iChallenge-PM	97.5	3.5
XProtoNet [11]	iChallenge-PM	98.25	3.3
DProtoNet(ours)	iChallenge-PM	98.5	19.7

Table 2: Comparison results on medical datasets.

Baselines. The interpretable neural networks ProtoPNet [2], NP-ProtoPNet [25], Gen-ProtoPNet [24], XProtoNet [11] and the non-interpretable backbone networks ResNet50 [9], VGG19 [23], DenseNet121 [10] are used as baselines to compare the accuracy with our proposed model.

We adopt the recent state-of-the-art saliency map methods Grad-CAM [21], Grad-CAM++ [1], Score-CAM [29], Ablation-CAM [19], interpretable neural networks ProtoPNet [2], NP-ProtoPNet [25], Gen-ProtoPNet [24], XProtoNet [11] generated class activation maps as baselines comparison with class activation maps generated by our model for Localization and Recognition performance.

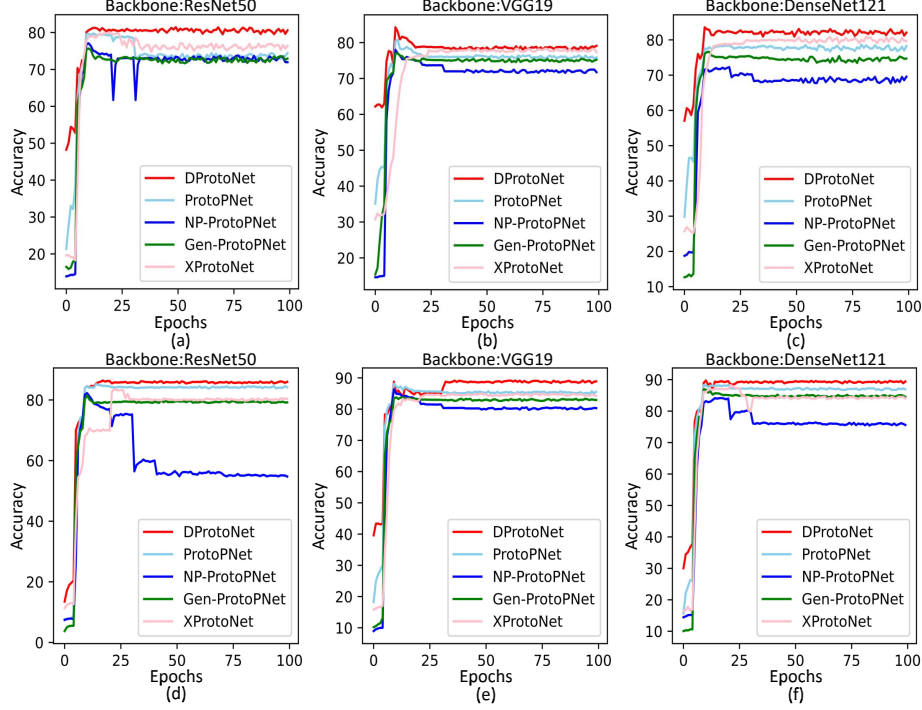


Figure 5: Comparison of training stage accuracy.

4.2 Evaluation

We test the performance of the model on the following nine evaluation metrics: Accuracy [25], Dice Coefficient (DICE) [13], IOU [13], PPV [13], Sensitivity [13], Average Drop (AD) [1], Average Increase (AI) [1], Deletion Scores (D) [18], Insertion Scores (I) [18].

Note: the TP , TN , FP , FN are true positive, true negative, false positive, false negative respectively, see [25]. $DICE = \frac{2TP}{FP+2TP+FN}$, $IOU = \frac{TP}{FP+TP+FN}$, $PPV = \frac{TP}{TP+FP}$, $Sensitivity = \frac{TP}{TP+FN}$ and $Accuracy = \frac{\text{number of correct predictions}}{\text{total number of cases}} = \frac{TP+TN}{TP+TN+FP+FN}$.

$AD = \sum_{i=1}^N \frac{100 \max(0, Y_i^c - O_i^c)}{Y_i^c}$, $AI = \sum_{i=1}^N \frac{Sign(Y_i^c < O_i^c)}{N}$. Y_i^c and O_i^c denotes the prediction score of class c in the original image i and explained map respectively. We removed certain percentile pixels of the original image to generate an explained map. $Sign(\cdot)$ is an indicator function, 1 if true, otherwise 0. D and I measures are the deletion and insertion of pixels from the original image in descending order of CAM activation value, respectively, and generate the area under the probability curve (AUC) described by the predicted probability result of the deleted or inserted image.

We generate the CAM as 0-1 binary mask according to a percentage thresh-

Backbone	Datasets	DProtoNet	Baseline
ResNet50	CUB200-2011	80.9	81.2
VGG19	CUB200-2011	77.9	75.5
DenseNet121	CUB200-2011	81.3	80.6
ResNet50	Stanford Cars	86.5	86.3
VGG19	Stanford Cars	89.2	88.6
DenseNet121	Stanford Cars	89.3	89.8
ResNet50	RSNA	82.2	79.6
VGG19	RSNA	79.3	78.2
DenseNet121	RSNA	80.6	79.9
ResNet50	iChallenge-PM	98.5	98.75
VGG19	iChallenge-PM	98.25	98.5
DenseNet121	iChallenge-PM	98.75	98.5

Table 3: Accuracy comparison on above four datasets.

old. We calculate Dice Coefficient, IOU, PPV, Sensitivity with the segmentation foreground or bounding box of the image to measure the Localization [29] ability of the CAM. We use AD, AI, D, I to measure the Recognition [29] ability of the CAM, and accuracy to measure the classification performance of the model.

4.3 Experimental Details

We set 10 prototypes for each class. Each image is rotated, perspective, sheared, and distorted to generate augmented images. All the images are cropped to 224×224 . Shaping network consist of two 1×1 convolutional layers with ReLU activation between them. Hyperparameters are derived using five-fold cross-validation, $\alpha = 0.5$, $\beta = 0.3$, $\gamma = 3$, $\tau = 0.5$, $\lambda_1 = 0.8$, $\lambda_2 = -0.08$, $\lambda_3 = 1e - 4$, $\epsilon = 1e - 12$, $D = 10$, $\{d_i\}_i^{10}$, $d_i \in R^{a_i \times b_i \times 1}$, $a_i = b_i = 5 + i$, $\eta_i = 10$, $i \in \{1, 2, \dots, 10\}$. The number of feature masks is 240. We use the Adam optimizer, the learning rates of backbone layer f_b , shape layer f_a , prototype activation layer g_p , and last layer f_h in the DProtoNet are set to $1e - 4$, $3e - 3$, $3e - 3$, $1e - 4$. The parameters of the network with ResNet50 [9], VGG19 [23], DenseNet121 [10] as the backbone are initialized to the values pre-trained on ImageNet [4]. The prototype channels is 512, batch is 60. Each masks vector is trained for 800 iterations. The initial stage is the first 5 epochs. After that, it is a joint stage, and the prototype update is performed every 10 epochs. In examining the Sensitivity [13], the binary mask threshold are set to the top 50% on the RSNA [30] and iChallenge-PM [7] datasets. In examining the Dice Coefficient [13], IOU [13], PPV [13] and Sensitivity [13], the binary mask thresholds are set to the top 80% on the CUB200-2011 [28].

Backbone	M=1	M=10	M=20	M=40
ResNet50 [9]	80.5	80.6	80.8	80.9
VGG19 [23]	77.5	77.7	77.8	77.9
DenseNet121 [10]	80.9	81.1	81.2	81.3

Table 4: Comparison of multi-image prototype learning.

4.4 Network Classification Performance

Comparing with Interpretable Networks. We compare the accuracy of DProtoNet with recent interpretable models. Table 1 shows that DProtoNet achieves state-of-the-art accuracy on ResNet50, VGG19 and DenseNet121 backbones on general datasets. As show in Table 2, we compare the accuracy and sensitivity on each model with ResNet50 as backbone. On the RSNA dataset, the accuracy of DProtoNet is 5.1% higher than that of the previous state-of-the-art model, and the sensitivity is 4.2% higher. On the iChallenge-PM dataset, DProtoNet outperforms previous models in both accuracy and sensitivity. DProtoNet has good accuracy for pathological images, and the decision regions it gives can well localize the real pathological regions. The reasoning process of DProtoNet complies with the process of “diagnosed disease based on pathological features found”, which is interpretable and can be recognized by clinicians. Figure 5 shows the variation in accuracy for each model trained on the bird and car datasets. (a), (b), (c) and (d), (e), (f) are the results on the bird and car datasets, respectively. DProtoNet converges faster than other models, and it achieves the best accuracy. All other interpretable networks suffer from accuracy degradation after performing the prototype update operation. After DProtoNet performs the prototype update, the classification performance of the network is almost not degraded, and the accuracy of the network is stable. This is because DProtoNet retains the interpretable inference process, but does not set a specific structure for the prototype, so that the values of the network will not mutate after the prototype is updated.

Comparison with Backbone Networks. Table 3 shows the comparison of accuracy of DProtoNet and its backbone network ResNet50, VGG19 and DenseNet121 on four datasets. The accuracy of DProtoNet is almost comparable to the classification performance of the backbone network on some datasets, and the performance on other datasets exceeds the accuracy of the backbone network. DProtoNet achieves interpretability without degrading its accuracy. DProtoNet extracts the global information of the feature map by using the unrestricted feature mask with strong expressive ability, and retains the fitting ability of the backbone as much as possible, so that the accuracy of DProtoNet can be comparable to that of the backbone network. DProtoNet treats the introduced backbone network as a black box and does not modify the internal architecture of the encoder network, so it can be widely applied to existing networks.

Method	AD	AI	D	I	DICE	IOU	PPV	Sensitivity
Grad-CAM [21]	27.8	14.2	0.134	0.339	0.288	0.186	0.292	0.336
Grad-CAM++ [1]	67.3	3.7	0.078	0.359	0.476	0.338	0.465	0.557
Score-CAM [29]	44.5	13.2	0.088	0.391	0.409	0.284	0.411	0.468
Ablation-CAM [19]	82.4	4.9	0.286	0.312	0.231	0.151	0.232	0.265
ProtoPNet [2]	75.1	3.2	0.038	0.349	0.527	0.373	0.509	0.639
NP-ProtoPNet [25]	45.7	11.5	0.161	0.271	0.071	0.044	0.076	0.075
Gen-ProtoPNet [24]	55.2	15.9	0.135	0.284	0.287	0.178	0.292	0.324
XProtoNet [11]	76.1	4.7	0.121	0.292	0.415	0.273	0.403	0.492
DProtoNet(ours)	17.5	21.1	0.028	0.709	0.548	0.391	0.531	0.651
ResNet50 $\uparrow\uparrow$, DenseNet121 $\downarrow\downarrow$ (backbone)								
Grad-CAM [21]	49.3	12.8	0.148	0.563	0.319	0.205	0.311	0.449
Grad-CAM++ [1]	71.3	4.6	0.045	0.315	0.521	0.365	0.509	0.607
Score-CAM [29]	37.5	13.9	0.091	0.632	0.466	0.329	0.461	0.541
Ablation-CAM [19]	89.6	2.5	0.127	0.185	0.254	0.163	0.254	0.294
ProtoPNet [2]	31.2	16.9	0.056	0.631	0.289	0.183	0.244	0.519
NP-ProtoPNet [25]	90.2	1.4	0.424	0.211	0.364	0.232	0.312	0.612
Gen-ProtoPNet [24]	60.2	11.9	0.161	0.261	0.298	0.186	0.298	0.342
XProtoNet [11]	31.8	17.3	0.102	0.617	0.397	0.256	0.389	0.473
DProtoNet(ours)	15.2	19.8	0.041	0.745	0.626	0.471	0.619	0.738

Table 5: Evaluated results on Recognition and Localization.

Evaluation of Multi-image Prototype Learning. Table 4 shows the accuracy of DProtoNet learned on the bird dataset [28] with ResNet50, VGG19 and DenseNet121 as backbones mixed with different numbers of M images as prototypes. M=1 indicates the single-image prototype learning method used by the previous models [2, 25, 24, 11]. As M increases, the network accuracy is higher. This method can learn prototypes generally, which improves the accuracy of the prototype-based interpretable network.

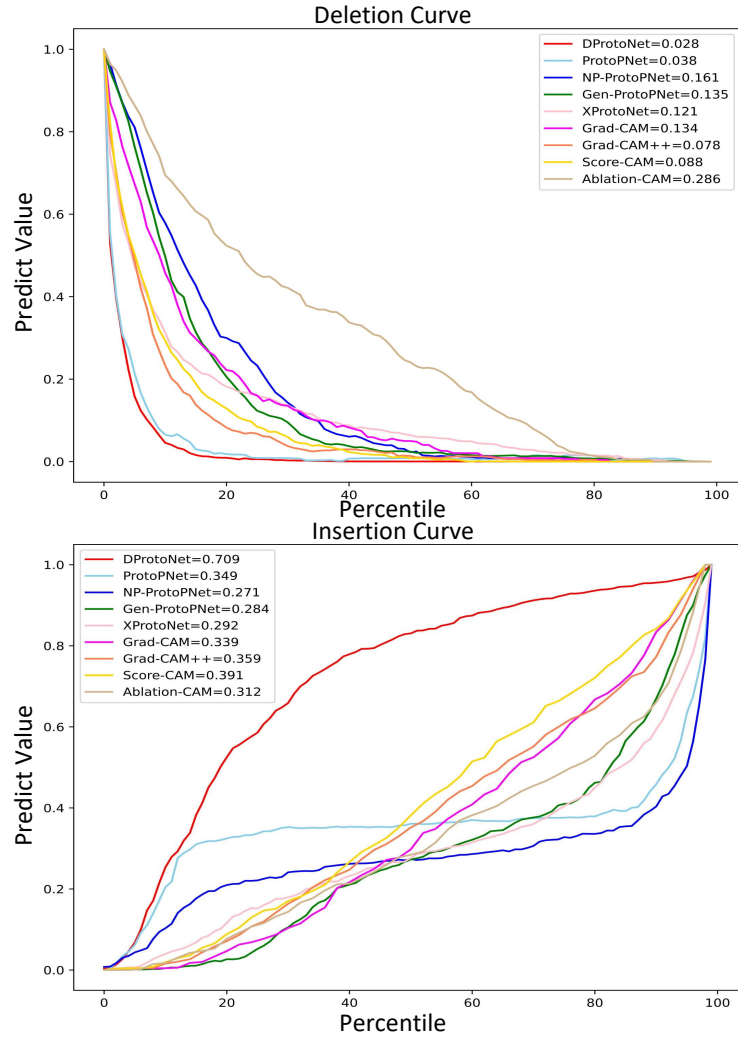


Figure 6: Deletion and Insertion curves of the above methods.


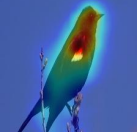






Prototype image	Prototype (in saliency map)	Input image	Find similarity prototype	Similarity Score	Class connection	Logits
				6.935	×	1.231 = 8.537
				5.167	×	1.107 = 5.720

Figure 7: DProtoNet inference process visualization.

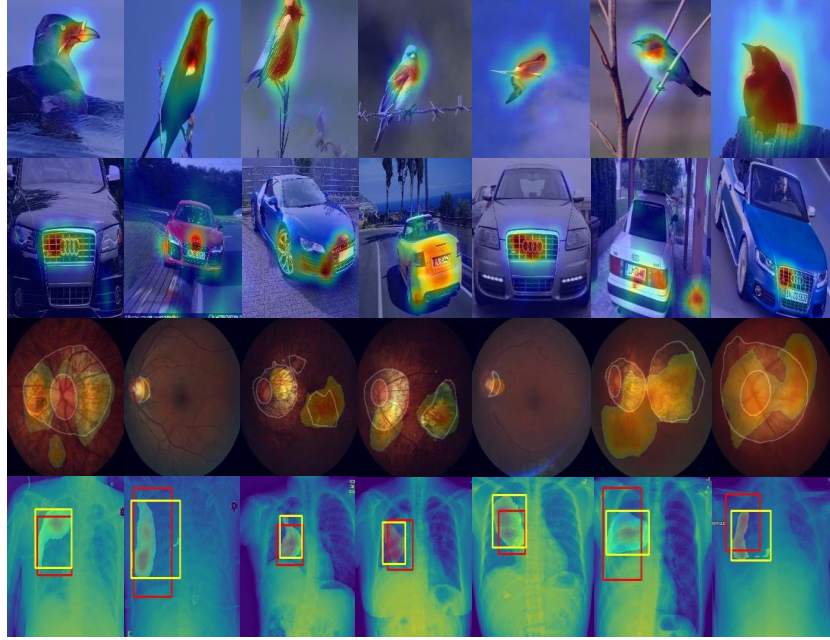


Figure 8: Visualization of decision regions.

4.5 Network Interpretability

Evaluation of Recognition and Localization. As shown in Table 5, we compare the performance of the CAM generated by MDM decoder for DProtoNet and the CAM generated by other methods on the eight evaluation indicators Average Drop, Average Increase, Deletion Score, Insertion Score, Dice Coefficient, IOU, PPV and Sensitivity. DProtoNet with ResNet50 as backbone

has improved by 37.1%, 32.7%, 26.3%, 81.3%, 3.9%, 4.8%, 4.3% and 1.9% respectively compared with the previous state-of-the-art model; DProtoNet with DenseNet121 as the backbone has improved by 51.3%, 14.5%, 8.9%, 17.9%, 20.2%, 29.1%, 21.6% and 20.6% respectively compared with the previous state-of-the-art model. CAM generated by MDM decoder achieves the state of the art in Localization and Recognition. Figure 6 shows that the probability curve corresponding to the CAM generated by DProtoNet with ResNet50 as backbone through the MDM decoder has the sharpest degree of change, which shows that DProtoNet can focus on the most meaningful regions for the classification. The CAM generated by MDM decoder has good interpretability.

Visualization. Figure 7 shows a visualization of the inference process of DProtoNet, which makes a decision by finding the prototype image that is most similar to the input image and comparing the similarity between the input image and the prototype image in the decision region. This is in line with our expectations for the DProtoNet inference process. Figure 8 visualizes the decision regions found by MDM decoder when predicting various images. In bird and car images, the CAM generated by MDM decoder is represented by the red to blue area. From blue to red, activation increases and network attention increases. The white-enclosed area in the iChallenge-PM images represents the pathological area that is the ground truth. In the RSNA images, the red box represents the real lesion area, and the yellow box represents the bounding box of lesion area found by MDM decoder. Figure 8 shows that the decision region found by MDM decoder is close to the real decision region, which is similar to the decision basis of human search. The DProtoNet is both interpretable for the inference process and can accurately tell people its decision basis.

5 Conclusion

In this paper, we propose an interpretable network, DProtoNet, which is able to generalize the learning and extraction of prototypes. DProtoNet treats the introduced network as a black box, so it can be universally applied to existing networks. We propose a general and powerful method, the MDM decoder, which is used to generate saliency maps to represent the decision basis of DProtoNet. The DProtoNet remove the mutual constraint between accuracy and interpretability. It can make the network interpretable while preserving the accuracy of the network. Experimental results show that the accuracy of our network outperforms other interpretable neural networks on the four datasets, is comparable to the performance of the backbone network, and has a huge improvement in interpretability. We wish this work to pave the way for future research and applications on explainable neural networks.

References

- [1] Aditya Chattopadhyay, Anirban Sarkar, Prantik Howlader, and Vineeth N Balasubramanian. Grad-cam++: Generalized gradient-based visual explanations for deep convolutional networks. In *2018 IEEE winter conference on applications of computer vision (WACV)*, pages 839–847. IEEE, 2018.
- [2] Chaofan Chen, Oscar Li, Daniel Tao, Alina Barnett, Cynthia Rudin, and Jonathan K Su. This looks like that: deep learning for interpretable image recognition. *Advances in neural information processing systems*, 32, 2019.
- [3] Jianbo Chen, Le Song, Martin Wainwright, and Michael Jordan. Learning to explain: An information-theoretic perspective on model interpretation. In *International Conference on Machine Learning*, pages 883–892. PMLR, 2018.
- [4] Jia Deng, Wei Dong, Richard Socher, Li-Jia Li, Kai Li, and Li Fei-Fei. Imagenet: A large-scale hierarchical image database. In *2009 IEEE conference on computer vision and pattern recognition*, pages 248–255. Ieee, 2009.
- [5] Alexey Dosovitskiy, Lucas Beyer, Alexander Kolesnikov, Dirk Weissenborn, Xiaohua Zhai, Thomas Unterthiner, Mostafa Dehghani, Matthias Minderer, Georg Heigold, Sylvain Gelly, et al. An image is worth 16x16 words: Transformers for image recognition at scale. *arXiv preprint arXiv:2010.11929*, 2020.
- [6] Ruth C Fong and Andrea Vedaldi. Interpretable explanations of black boxes by meaningful perturbation. In *Proceedings of the IEEE international conference on computer vision*, pages 3429–3437, 2017.
- [7] Huazhu Fu, Fei Li, José Ignacio Orlando, Hrvoje Bogunovic, Xu Sun, Jingan Liao, Yanwu Xu, Shaochong Zhang, and Xiulan Zhang. Palm: Pathologic myopia challenge. *IEEE Dataport*, 2019.
- [8] Peter Hase, Chaofan Chen, Oscar Li, and Cynthia Rudin. Interpretable image recognition with hierarchical prototypes. In *Proceedings of the AAAI Conference on Human Computation and Crowdsourcing*, volume 7, pages 32–40, 2019.
- [9] Kaiming He, Xiangyu Zhang, Shaoqing Ren, and Jian Sun. Deep residual learning for image recognition. In *Proceedings of the IEEE conference on computer vision and pattern recognition*, pages 770–778, 2016.
- [10] Gao Huang, Zhuang Liu, Laurens Van Der Maaten, and Kilian Q Weinberger. Densely connected convolutional networks. In *Proceedings of the IEEE conference on computer vision and pattern recognition*, pages 4700–4708, 2017.

- [11] Eunji Kim, Siwon Kim, Minji Seo, and Sungroh Yoon. Xprotonet: diagnosis in chest radiography with global and local explanations. In *Proceedings of the IEEE/CVF conference on computer vision and pattern recognition*, pages 15719–15728, 2021.
- [12] Jonathan Krause, Michael Stark, Jia Deng, and Li Fei-Fei. 3d object representations for fine-grained categorization. In *Proceedings of the IEEE international conference on computer vision workshops*, pages 554–561, 2013.
- [13] Issam Laradji, Pau Rodriguez, Oscar Manas, Keegan Lensink, Marco Law, Lironne Kurzman, William Parker, David Vazquez, and Derek Nowrouzezahrai. A weakly supervised consistency-based learning method for covid-19 segmentation in ct images. In *Proceedings of the IEEE/CVF Winter Conference on Applications of Computer Vision*, pages 2453–2462, 2021.
- [14] Oscar Li, Hao Liu, Chaofan Chen, and Cynthia Rudin. Deep learning for case-based reasoning through prototypes: A neural network that explains its predictions. In *Proceedings of the AAAI Conference on Artificial Intelligence*, volume 32, 2018.
- [15] Ze Liu, Yutong Lin, Yue Cao, Han Hu, Yixuan Wei, Zheng Zhang, Stephen Lin, and Baining Guo. Swin transformer: Hierarchical vision transformer using shifted windows. In *Proceedings of the IEEE/CVF International Conference on Computer Vision*, pages 10012–10022, 2021.
- [16] Zhuang Liu, Hanzi Mao, Chao-Yuan Wu, Christoph Feichtenhofer, Trevor Darrell, and Saining Xie. A convnet for the 2020s. In *Proceedings of the IEEE/CVF Conference on Computer Vision and Pattern Recognition*, pages 11976–11986, 2022.
- [17] Cristiano Patrício, João C Neves, and Luís F Teixeira. Explainable deep learning methods in medical diagnosis: A survey. *arXiv preprint arXiv:2205.04766*, 2022.
- [18] Vitali Petsiuk, Abir Das, and Kate Saenko. Rise: Randomized input sampling for explanation of black-box models. *arXiv preprint arXiv:1806.07421*, 2018.
- [19] Harish Guruprasad Ramaswamy et al. Ablation-cam: Visual explanations for deep convolutional network via gradient-free localization. In *Proceedings of the IEEE/CVF Winter Conference on Applications of Computer Vision*, pages 983–991, 2020.
- [20] Cynthia Rudin. Stop explaining black box machine learning models for high stakes decisions and use interpretable models instead. *Nature Machine Intelligence*, 1(5):206–215, 2019.

- [21] Ramprasaath R Selvaraju, Michael Cogswell, Abhishek Das, Ramakrishna Vedantam, Devi Parikh, and Dhruv Batra. Grad-cam: Visual explanations from deep networks via gradient-based localization. In *Proceedings of the IEEE international conference on computer vision*, pages 618–626, 2017.
- [22] Avanti Shrikumar, Peyton Greenside, and Anshul Kundaje. Learning important features through propagating activation differences. In *International conference on machine learning*, pages 3145–3153. PMLR, 2017.
- [23] Karen Simonyan and Andrew Zisserman. Very deep convolutional networks for large-scale image recognition. *arXiv preprint arXiv:1409.1556*, 2014.
- [24] Gurmail Singh and Kin-Choong Yow. An interpretable deep learning model for covid-19 detection with chest x-ray images. *Ieee Access*, 9:85198–85208, 2021.
- [25] Gurmail Singh and Kin-Choong Yow. These do not look like those: An interpretable deep learning model for image recognition. *IEEE Access*, 9:41482–41493, 2021.
- [26] Mukund Sundararajan, Ankur Taly, and Qiqi Yan. Axiomatic attribution for deep networks. In *International conference on machine learning*, pages 3319–3328. PMLR, 2017.
- [27] Christian Szegedy, Wei Liu, Yangqing Jia, Pierre Sermanet, Scott Reed, Dragomir Anguelov, Dumitru Erhan, Vincent Vanhoucke, and Andrew Rabinovich. Going deeper with convolutions. In *Proceedings of the IEEE conference on computer vision and pattern recognition*, pages 1–9, 2015.
- [28] Catherine Wah, Steve Branson, Peter Welinder, Pietro Perona, and Serge Belongie. The caltech-ucsd birds-200-2011 dataset. 2011.
- [29] Haofan Wang, Zifan Wang, Mengnan Du, Fan Yang, Zijian Zhang, Sirui Ding, Piotr Mardziel, and Xia Hu. Score-cam: Score-weighted visual explanations for convolutional neural networks. In *Proceedings of the IEEE/CVF conference on computer vision and pattern recognition workshops*, pages 24–25, 2020.
- [30] Xiaosong Wang, Yifan Peng, Le Lu, Zhiyong Lu, Mohammadhadi Bagheri, and Ronald M Summers. Chestx-ray8: Hospital-scale chest x-ray database and benchmarks on weakly-supervised classification and localization of common thorax diseases. In *Proceedings of the IEEE conference on computer vision and pattern recognition*, pages 2097–2106, 2017.
- [31] Hao Yuan, Lei Cai, Xia Hu, Jie Wang, and Shuiwang Ji. Interpreting image classifiers by generating discrete masks. *IEEE Transactions on Pattern Analysis and Machine Intelligence*, 2020.

- [32] Bolei Zhou, Aditya Khosla, Agata Lapedriza, Aude Oliva, and Antonio Torralba. Learning deep features for discriminative localization. In *Proceedings of the IEEE conference on computer vision and pattern recognition*, pages 2921–2929, 2016.